catalysts

MDPI

Article

Bulk, Surface and Interface Promotion of Co_3O_4 for the Low-Temperature N_2O Decomposition Catalysis

Sylwia Wójcik, Gabriela Grzybek, Paweł Stelmachowski, Zbigniew Sojka and Andrzej Kotarba *

Faculty of Chemistry, Jagiellonian University, Gronostajowa 2, 30-387 Krakow, Poland; sylwia.gudyka@doctoral.uj.edu.pl (S.W.); g.grzybek@uj.edu.pl (G.G.); pawel.stelmachowski@uj.edu.pl (P.S.); sojka@chemia.uj.edu.pl (Z.S.)

* Correspondence: ak@uj.edu.pl; Tel.: +48-12-686-2509

Received: 28 November 2019; Accepted: 27 December 2019; Published: 30 December 2019

Abstract: Nanocrystalline cobalt spinel has been recognized as a very active catalytic material for N_2O decomposition. Its catalytic performance can be substantially modified by proper doping with alien cations with precise control of their loading and location (spinel surface, bulk, and spinel-dopant interface). Various doping scenarios for a rational design of the optimal catalyst for low-temperature N_2O decomposition are analyzed in detail and the key reactivity descriptors are identified (content and topological localization of dopants, their redox vs. non-redox nature and catalyst work function). The obtained results are discussed in the broader context of the available literature data to establish general guidelines for the rational design of the N_2O decomposition catalyst based on a cobalt spinel platform.

Keywords: cobalt spinel; nanocrystals; bulk and surface promoters; interface; nitrous oxide; reactivity descriptors

1. Introduction

The reaction of low-temperature catalytic nitrous oxide decomposition has been investigated over a variety of active phases, such as noble metals, metal oxides, zeolites, and perovskites [1–5]. Extensive research revealed cobalt spinel as one of the most active phases for the process of N_2O decomposition (deN_2O process) [6–8]. The catalytic performance of Co_3O_4 can be significantly enhanced by tuning the composition and crystal morphology (controlled faceting) [9–11]. Optimization of the chemical composition of the cobalt spinel via controlled addition of dopants can result in a spectacular improvement of catalytic performance. The structural and surface promotional effects have been established and well documented so far [6,12,13]. Furthermore, optimized synthesis procedures have been developed to obtain Co_3O_4 nanocrystals with the most favorable cubic-like morphology with a high exposition of the (100) planes—the most active in N_2O decomposition [14,15].

A literature survey and our previous studies indicate that the structure of the cobalt spinel active phase can be doped with various metal cations [14–18]. Among them, the most promising effect for the deN_2O reaction has been reported for Zn, Ni, Pb and Bi addition [19–22]. The surface promotion through the decoration of cobalt spinel with s-block [22,23] and rare earth [24–27] elements has also been proved to be particularly beneficial for nitrous oxide decomposition reaction. It should be emphasized, however, that only a precisely optimized amount of a specific dopant ensures a substantial promotional effect and the resultant enhancement of the cobalt spinel performance [28]. The promotional effect of alkali doping was found to be associated with the modification of the electronic properties of the cobalt spinel catalyst, where introducing alkali at the Co_3O_4 surface facilitates the electron transfer between the catalyst and the reactants [29]. So far, potassium is certainly the most widely applied dopant

due to its large promotional effect and low price. It was also found that in addition to the surface concentration, the nature of the counterion and thermally induced surface dynamics of potassium substantially influence the deN_2O reactivity, and should be taken into account for the evaluation of the catalyst long term stability [30,31].

The aim of this paper was to systematize and rationalize the effects of additives on the cobalt spinel catalytic performance in nitrous oxide decomposition using easily determinable reactivity descriptors. In order to delineate and characterize various classes of promotional effects of cobalt spinel, the catalytic results coming from our laboratory were discussed in the broader context of the relevant recent literature data.

2. Results

2.1. N_2O Performance of Promoted Cobalt Spinel-Based Catalysts

For the reliable comparison of cobalt spinel active phase dopants, systematic investigations were carried out in the same conditions. The results of screening deN_2O catalytic tests at the same conditions (Gas Hourly Space Velocity (GHSV) = 7000 h^{-1}) for various *s*-, *p*-, *d*-doped cobalt spinel are presented in Figure 1. The concentration of each of the promoters was priory optimized using the data from a wide percentage range. In Figure 1, the conversion profiles correspond to the following optimized concentrations of the Na (0.2 wt.%), K (0.4 wt.%), Cs (1.3 wt.%), Mg (12 wt.%), Al (31 wt.%), Pb (14 wt.%), Ni (17 wt.%), Zn (11 wt.%), and Ce (11 wt.%) dopants.

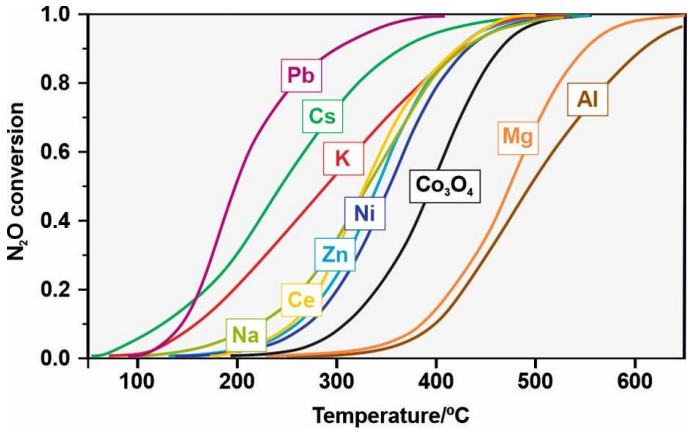

Figure 1. The N_2O conversion curves as a function of temperature for the bare and cobalt spinel-doped with Na, K, Cs, Mg, Al, Pb, Ni, Zn, and Ce, at specific optimal concentrations.

The presented data (Figure 1) clearly shows dramatic positive (promotional) and negative effects of dopants depending on their chemical nature. Whereas the addition of optimal concentrations of alkali metals (Na, K, Cs), transition metals (Zn, Ni), as well as Pb, Ce elements shifts the conversion curves to the lower temperatures, the presence of Mg and Al dopants significantly decrease the catalytic performance of cobalt spinel. Although the comparison of the relative catalytic activity is easy to conclude (Figure 1), an explanation of the origin of the doping effects is still not resolved definitely. This is caused by the fact that the promotional effect results not only from the nature and concentration of the dopants but also from their surface/bulk/interface localization (vide infra). Based on our research and the literature data on Co_3O_4 properties, structure, and morphology, the applied dopants can be classified into the following three groups: surface (Na, K, Cs), bulk (Zn, Ni, Mg, Al) and interfacial (PbO_2, CeO_2) promoters. The presented classification was consequently applied hereafter not only to explain the specific functioning of the particular dopant but also for the rational design of the effective deN_2O catalysts.

2.2. Physicochemical Characterization

The physicochemical characterization of the investigated bare and doped cobalt spinel-based catalysts was performed with the use of several experimental methods: X-ray diffraction (XRD), Raman Spectroscopy (RS), specific surface area measurements by means of Brunauer, Emmett and Teller (BET) method, X-ray photoelectron spectroscopy (XPS), hydrogen-temperature programmed reduction (H_2-TPR) and transmission electron microscopy (TEM). In this section, for the sake of conciseness, only exemplary results are presented for each of the three distinguished generic classes of the promoters. They illustrate how the localization of the promoter can be revealed.

2.2.1. Bulk Promoted Catalysts

The AB_2O_4 normal spinel *Fd3m* structure (assumed for Co_3O_4) contains the divalent A cations in the tetrahedral positions and the trivalent B cations in the octahedral positions. The flexible structure of Co_3O_4 enables a wide-ranging substitution of both Co^{2+} or Co^{3+} cations while preserving the overall spinel structure (Figure 2a,b). In Figure 2a–d, the results for the selected bulk promoters, Zn and Al, on the cobalt spinel active phase are presented. Analysis of the diffractograms (Figure 2a) indicates the preserved structural integrity of a cobalt spinel phase and the lack of the segregated zinc of aluminum oxides. Characteristic maxima located at 2Θ = 19.1 (111), 31.3 (220), 36.9 (311), 38.2 (222), 44.9 (400), 55.3 (422), 59.5 (511), 65.4 (440), 76.8 (533), 77.3 (622) were recognized as typical lines of a single Co_3O_4 phase (ICSD—69378).

The complementary analysis of the phase composition of the investigated materials was carried out by Raman spectroscopy, which as a local structure probe is more sensitive to the presence of possible spurious phases than the XRD technique. All of the collected RS spectra confirmed the sole presence of the cobalt spinel phase of high crystallinity (Figure 2b). Five characteristic Co_3O_4 vibrational bands assigned to the F_{2g}, E_g, F_{2g}, $F_{2g,}$ and A_{1g} modes can be clearly distinguished at the specific frequencies 196, 482, 523, 618 and 691 cm^{-1}, respectively. There are also no visible changes in the case of the potassium doped catalyst (red curve), which confirms surface localization of the alkali promoter only. However, the spectrum of zinc promoted cobalt spinel catalyst (Figure 2b, blue line) clearly shows a structural modification of the parent Co_3O_4. The observed splits and shifts of the Raman bands indicated the incorporation of Zn^{2+} ions into the tetrahedral and Al^{3+} into the octahedral interstitials.

The H_2-TPR profiles of the bare Co_3O_4 and bulk Al-promoted catalysts are shown in Figure 2c. In the case of undoped cobalt spinel, two overlapping reduction maxima can be recognized: a low-temperature band at 300–400 °C attributed to the reduction of Co^{3+} to Co^{2+}, and a high-temperature one assigned to the reduction of Co^{2+} to the metallic cobalt. Partial substitution of cobalt by aluminum cations leads to a decrease in the overall reducibility of the spinel catalyst and pronounced shift of both reduction maxima. It is particularly important for the onset of the low-temperature reduction, which is considered as a simple descriptor of the catalyst redox behavior [32], often associated with the catalytic performance.

The typical morphology of the reference catalyst, Co_3O_4, obtained by the most common precipitation method is presented in Figure 2d,e. The TEM images clearly reveal the rhombicuboctahedral shape of the spinel nanoparticles with the size in the range of 30–50 nm. The inversed Wulff construction for the undoped and doped nanocrystal of cobalt spinel catalysts show changes in the abundance of the exposed (111), (110) and (100) planes (Figure 2f). Among them, the (100) facet is the most desirable because of the high concentration of the octahedral cobalt cations Co^{3+}, being recognized as the active sites of the N_2O decomposition reaction [32]. The evoked examples clearly illustrate also how, by suitable bulk doping, the shape of the cobalt spinel nanocrystals can be engineered towards the required morphology for the highest deN_2O performance.

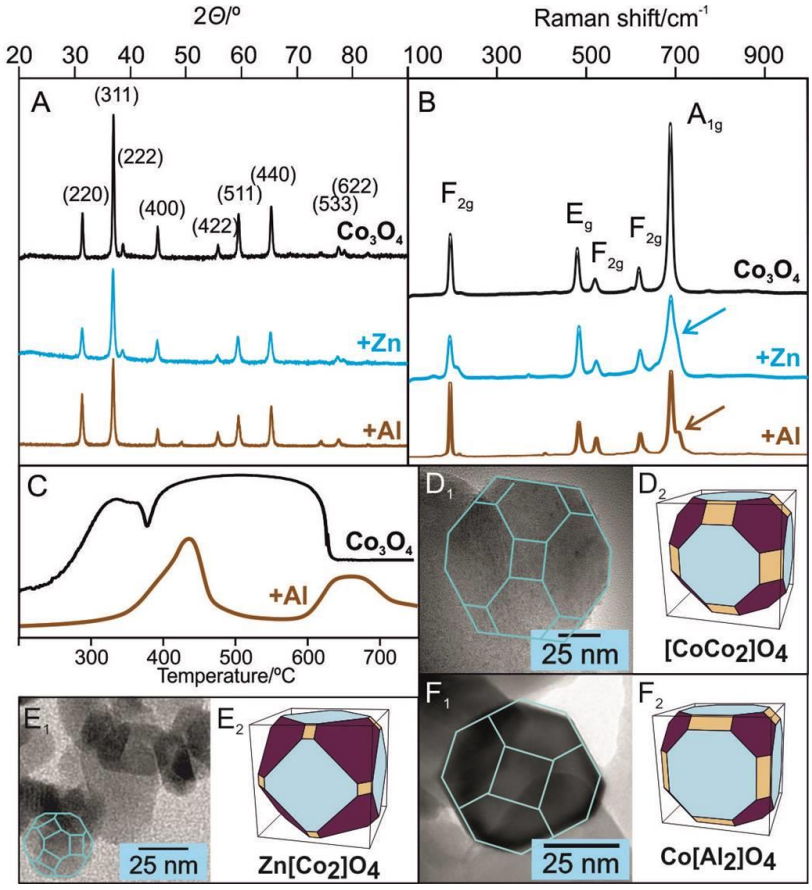

Figure 2. Physicochemical characterization of bulk-promoted cobalt spinel catalysts (**A**–**C**); transmission electron microscopy (TEM) image of Co_3O_4 nanocrystals (**D_1**,**E_1**,**F_1**) and models of exposed facets (**D_2**,**E_2**,**F_2**): (111), (110), (100) marked by blueberry, peach, and pale cyan colors, respectively (**F**) [33].

Depending on the dopants nature, they can be located in the tetrahedral (A) or octahedral sites (B), as schematically depicted in Figure 3. It should be noted that the real spinel catalyst is featured by a certain extent of the inversion (where 2+ and 3+ cations switch their places), especially for high doping levels and high temperatures. As implied by the XRD and Raman spectroscopic studies, the introduction of divalent Mg^{2+} or Zn^{2+} cations into Co_3O_4 leads to their preferential localization in the A sites, while trivalent cations such as Al^{3+} or Cr^{3+} used as doping cations localize mostly in the B sites [34–37]. There are also several cations (Fe, Ni, Mn) which may change their localization in the spinel framework depending on the oxidation state and loading (Figure 3) [38]. The locus of the doping cations, however, has a more prominent influence on their catalytic deN_2O activity than their electronic configuration. The transition metal cations, such as Ni^{2+} or Zn^{2+} (redox-active cations), introduced into the cobalt spinel structure induce promoting effect and enhance the rate of N_2O decomposition. Doping of Co_3O_4 with *s* or *p* group cations, such as Mg^{2+} or Al^{3+} (redox-inert cations), leads to heavily deteriorated catalytic activity. These effects are illustrated in Figure 1, where the exemplary conversion curves are shifted toward higher and lower temperatures with respect to the Co_3O_4 reference depending on the dopant nature.

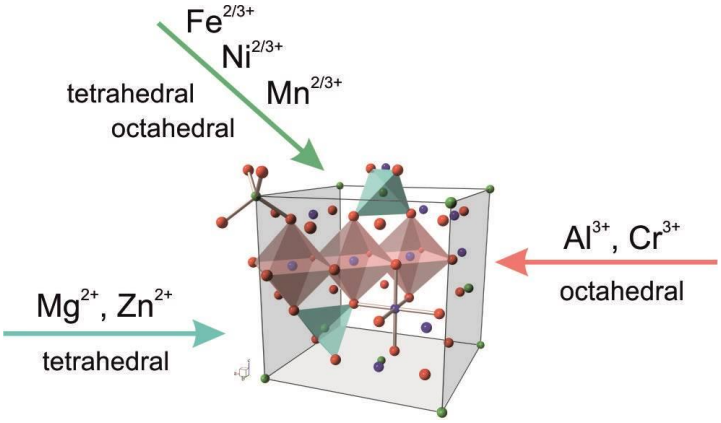

Figure 3. Schematic representation of possible localization sites for bulk promoters in the spinel structure.

It has been found, by the selective substitution of Co^{3+} by Al^{3+} and Co^{2+} by Mg^{2+}, that the trivalent Co ions located in the octahedral sites act as the active sites in N_2O decomposition, whereas the divalent cobalt ions located in the tetrahedral sites are distinctly less active [39]. Doping with the redox-active cations modifies the electronic properties of the cobalt spinel phase, as gauged by the work function change [33], with a strong impact on deN_2O performance. Indeed, the determined activation energies for Ni- and Zn-doped Co_3O_4 catalysts are slightly lower than for the pristine cobalt spinel (Table 1). In addition to the changes in the electronic properties, the structural doping with alien cations may influence the morphology of the cobalt spinel nanocrystals, and therefore their specific activity [33,40]. It should be noted that the value of activation energy (E_a) around 63 kJ mol^{-1}, determined here, is one of the minimal values for the undoped cobalt spinel catalysts. Changes in the Co_3O_4 catalysts surface state and nanocrystallite morphology into more irregular shapes usually bring about an increase of the E_a values. This can be explained i.a. due to the exposition of the higher Miller index crystal facets, which stabilize the intermediate oxygen species [41]. This hinders their recombination into O_2 gas-phase (closing step in the catalytic cycle), leading to an overall decrease of the catalytic activity [33,40].

Table 1. Activation energies for N_2O decomposition for selected bulk-doped Co_3O_4.

Sample	E_a/kJ mol^{-1}	SSA */m^2g^{-1}
Co_3O_4	63	30
$Zn_{0.4}Co_{2.6}O_4$	61	58
$Ni_{0.7}Co_{2.3}O_4$	60	53
$MgCo_2O_4$	71	6
$CoAl_2O_4$	117	34

* SSA—specific surface area.

2.2.2. Surface Promotion

In Figure 4a–c, the results of surface K and Cs promotion of the cobalt spinel active phase are presented. Analysis of the registered diffractograms (Figure 4a) indicates the sole presence of a cobalt spinel phase in the investigated catalysts. No important changes between diffractograms of pure spinel (black line) and surface-doped (red and green lines) active phases can be distinguished. For Raman spectroscopy, the collected spectra confirmed the presence of the cobalt spinel phase (see Figure 4b). There are no visible changes in the case of the potassium and cesium doped catalysts, which confirms only a surface localization of the alkali promoters.

The H_2-TPR profiles of the surface (K-Co_3O_4) promoted catalyst are shown in Figure 4c with the reference bare Co_3O_4. The reduction curve registered for the K-doped catalyst reveals a shift of the first stage reduction to the lower temperatures while the second maximum exhibits a similar profile in

comparison with the reference sample. In this case, the Co^{3+} and Co^{2+} reduction bands are not resolved, which is caused by the grain size and shape effects on the cobalt spinel reducibility (c.f. Figure 2 and Figure 7). It should be mentioned, however, that in this paper for each mode of promotion we always used the Co_3O_4 reference prepared from the same batch as the doped catalysts. This observation can be correlated with the improvement of the catalytic activity of the K-doped catalyst.

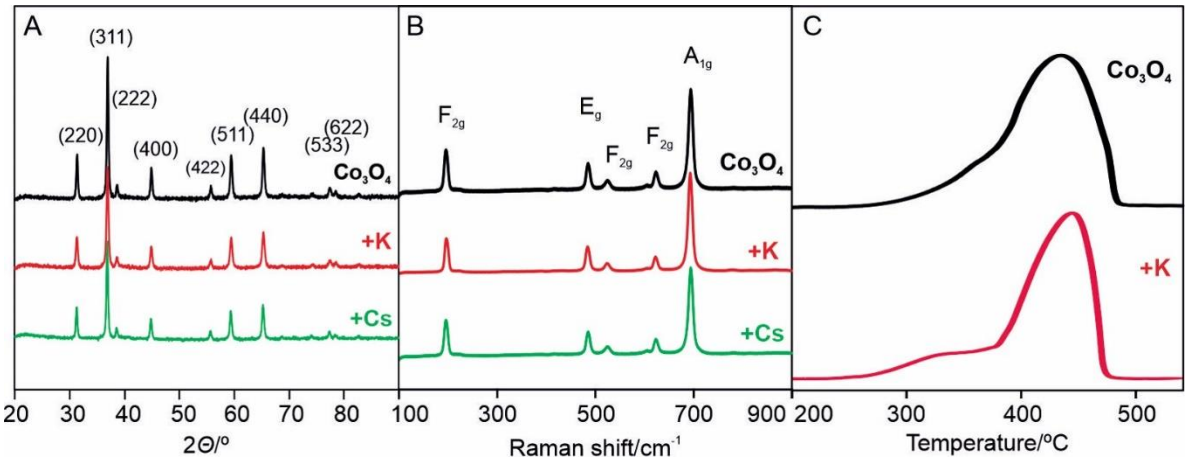

Figure 4. Physicochemical characterization of surface promoted cobalt spinel catalysts by X-ray diffraction (XRD) (**A**), Raman Spectroscopy (**B**) and temperature programmed reduction (TPR) (**C**) techniques.

In recent years, a significant effect of alkali doping on catalytic performance in the deN_2O reaction of a variety of metal oxides has been reported [13,29,42,43]. In particular, the activity of cobalt spinel has been found to be extremely sensitive to alkali doping. The decomposition of nitrous oxide over transition metal oxides may be represented by the cationic redox mechanism [44,45], in which all steps depend on the electronic properties of the catalyst surface. Therefore, the electronic nature of alkali doping of Co_3O_4 was examined by work function measurement with the dynamic condenser method (Kelvin method) [46]. As shown in Figure 5a,b, where the temperature of 50% conversion of N_2O decomposition is plotted against the catalyst work function changes ($\Delta\Phi$), both the potassium counter ion and the type of the doped alkali metal strongly influence the surface work function and the activity of cobalt spinel catalysts.

The effect of alkali counter ion was studied using different precursors varying the type of the counterion for the same alkali metal (K_2CO_3, KNO_3, CH_3COOK, KOH) and changing the alkali metal for the same anion (Li_2CO_3, Na_2CO_3, K_2CO_3, Rb_2CO_3, Cs_2CO_3). For both series, catalytic screening was performed at the same conditions. The highest beneficial effect observed for potassium carbonate was assigned to the highest surface dispersion and stability of the potassium promoter described in more detail in our previous paper [29]. The decrease of the half N_2O conversion temperature over the cobalt spinel catalyst upon potassium doping correlates strongly with the work function changes.

The alkali dopant nature enhances the spinel catalyst activity following the order of their ionic radius: Li << Na < Rb ≅ K < Cs (Figure 5b). Again, the deN_2O activity correlates well with the observed lowering of the spinel work function upon alkali doping, and the most active catalyst exhibits the lowest work function [13].

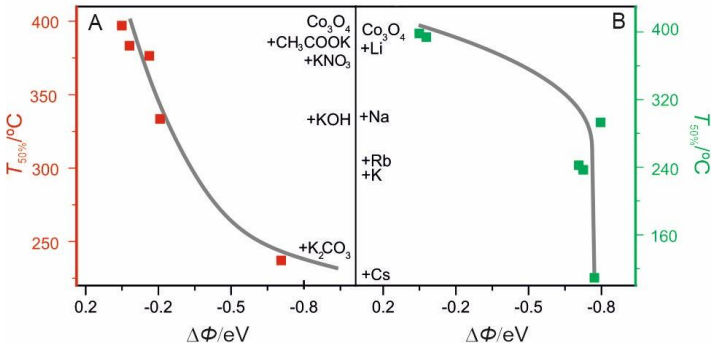

Figure 5. The catalytic activity represented by half conversion temperature of N_2O decomposition ($T_{50\%}$) against the catalyst work function changes for K-promoted cobalt spinel obtained with different potassium precursors (**A**) and cobalt spinel promoted with Li, Na, Rb, K, and Cs carbonates (**B**). The alkali concentration equals 2 atoms/nm^2 for all samples.

The optimization of alkali surface loading for the best potassium and cesium dopants was examined for the wide range of 0–8 atoms nm^{-2}. The half N_2O conversion temperatures of the K- and Cs-doped Co_3O_4 catalysts (impregnated with carbonates) are plotted against alkali loading in Figure 6a,c, and compared with the corresponding work function changes (Figure 6b,d). All the presented curves exhibit a non-monotonous behavior of the $T_{50\%}$ and Φ values with the minimum located at about 2–3 atoms nm^{-2} for K and Cs, respectively. The presented strong correlation between reactivity in the deN_2O process and the work function changes of the spinel catalysts clearly confirms the electronic character of the alkali promotion observed previously [13].

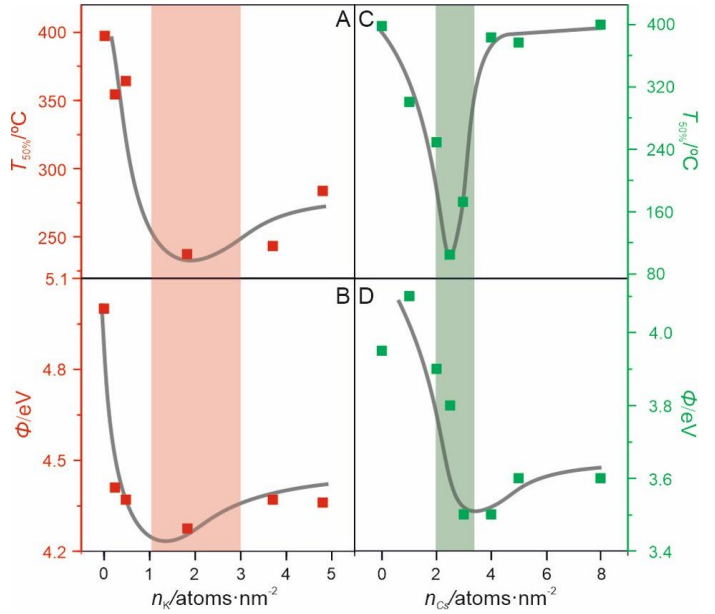

Figure 6. The half conversion temperature of N_2O ($T_{50\%}$) (**A**,**C**) and work function (Φ) (**B**,**D**) as a function of potassium (**A**,**B**) and cesium (**C**,**D**) loading introduced from a carbonate precursor.

The explanation of such a dramatic enhancement of cobalt spinel performance requires a mechanistic insight into the observable electronic phenomena [13]. Deposition of the small amounts of alkali metals with low ionization potential results in the formation of isolated surface dipoles [28]. Their presence, reducing surface potential, facilitates the electron exchange between the catalyst and N_2O (reduction step) and O^- (oxidation step) during the catalytic process. Indeed, according to the Topping model (Equation (1)), such a situation gives rise to the lowering of the interfacial potential [47],

favoring the electron transfer from the surface to the N_2O molecule and from O^- intermediates back to the surface.

$$\Delta\Phi = \frac{\mu}{\varepsilon_0}\cdot n_A\cdot\left(1+\frac{\kappa\cdot\alpha\cdot n_A^{2/3}}{4\cdot\pi\cdot\varepsilon_0}\right)^{-1}, \quad (1)$$

where $\Delta\Phi$ [eV] is the work function changes, n_A [m^{-2}] is the alkali promoter surface coverage, and $\kappa\cdot\alpha$ [$cm^2\ V^{-1}$] is the product of geometrical factor and polarizability of a promoter surface atom, which accounts for the depolarization effect. However, as the surface concentration of $K^{\delta+}$–O_{surf} dipoles increases and the dipoles become closer the depolarization effect reduces the surface potential lowering (Equation (1)). Such a model provides the rational account for the observed non-monotonous character of the promotion effect and a narrow range of the alkali loading where the promotional effect is the strongest as well. It also implies the crucial role of the doping level of the alkali promoter since, as presented in Figure 6, the optimal range is not only small but also different for each alkali cation.

2.2.3. Interface Promotion

The cobalt spinel active phase was promoted by cerium and lead, and characterized by XRD, Raman Spectroscopy and H_2 temperature-programmed reduction. The obtained data are collected in Figure 7. The diffractograms (panel A) indicate beside the prime cobalt spinel phase also the presence of minor oxide phases of CeO_2 and PbO_2 due to the segregated dopants. In the diffractogram of the Ce-doped catalyst (Figure 7a, yellow curve), the presence of Ce(IV) oxide was confirmed by the lines at a 2θ value of 28.6°, 33.2°, 47.5° and 56.4° corresponding to (111), (200), (220) and (311) planes of cubic ceria, respectively (ICSD—28753). On the other hand, reflexes posited at 28.8 (111), 32.0 (200), 47.9 (220) and 55.2 (311) confirm the segregation of the PbO_2 phase in the Pb-doped catalyst (Figure 7a, pink curve). In addition, the visibly broadened peaks characteristic for the Co_3O_4 phase, represent the significant decrease of the size of spinel crystals in both doped catalysts. The Raman spectra (panel B) of all samples are characteristic for Co_3O_4, implying that the spinel structure is not affected in an appreciable way upon the addition of such promoters. The comparison of H_2-TPR profiles of undoped and Pb-doped samples indicates almost unchanged shape and slight shift towards lower temperatures in the case of PbO_2-Co_3O_4 catalyst, caused by the lower size of its crystals. The shift of the TPR onset toward lower temperature upon Pb addition is consistent with the enhanced mobility of the interfacial oxygen (Figure 7c). The presented results, in-line with the previously reported data [48–50], reveal that for Ce and Pb-doped spinels the catalysts exhibit the characteristic two-phase morphology, where the small dopant oxide nanoparticles are spread over the cobalt spinel surface. Such an arrangement is featured by the formation of the reactive interface which has been shown as beneficial for the efficient N_2O decomposition reaction [48]. Owing to the oxygen mobility enhancement the role of the interface consists in the facilitation of the oxygen recombination step.

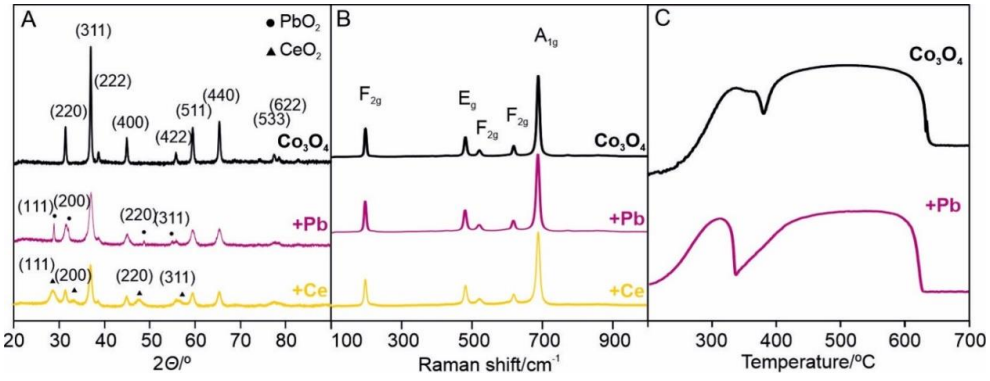

Figure 7. Physicochemical characterization of Pb- and Ce-doped Co_3O_4 based catalysts by XRD (**A**), Raman Spectroscopy (**B**) and TPR (**C**) techniques.

3. Discussion

Selected literature data and the results obtained in our laboratory for nitrous oxide decomposition over various cobalt spinel-based catalysts are collated in Table 2. They illustrate qualitatively the overall span of the bulk, surface and interface promotion effectiveness and the potential applicability of such materials as catalysts for low-temperature deN_2O. It should be noted, however, that due to various test conditions the reported $T_{50\%}$ values represent only a rough estimation of specific catalyst performance.

Table 2. Selected spinel-based catalysts deN_2O performance in terms of the temperature of 50% conversion of N_2O ($T_{50\%}$) at various feed composition and Gas Hourly Space Velocity (GHSV).

Catalyst	Conditions	$T_{50\%}$	Reference
Co_3O_4	5% N_2O, GHSV = 7000 h^{-1}	380	This work
Co_3O_4	0.5% N_2O, GHSV = 80,000 h^{-1}	475	[12]
Co_3O_4	0.1% N_2O, GHSV = 15,000 h^{-1}	340	[51]
$MgCo_2O_4$	5% N_2O, GHSV = 7000 h^{-1}	460	This work
$MgCo_2O_4$	0.5% N_2O, GHSV = 80,000 h^{-1}	440	[12]
$Co_{0.6}Fe_{2.4}O_4$	Pure N_2O, GHSV = 15,000 h^{-1}	160	[52]
Co_2FeO_4	5% N_2O, GHSV = 7000 h^{-1}	442	This work
$CoFe_2O_4$	0.5% N_2O, GHSV = 80,000 h^{-1}	580	[12]
$Zn_{0.36}Co_{2.64}O_4$	0.1% N_2O, GHSV = 15,000 h^{-1}	130	[51]
$Zn_{0.4}Co_{2.6}O_4$	5% N_2O, GHSV = 7000 h^{-1}	320	This work
$ZnCo_2O_4$	0.5% N_2O, GHSV = 80,000 h^{-1}	475	[12]
K-Co_3O_4	5% N_2O, GHSV = 7000 h^{-1}	235	This work
K-Co_3O_4	0.05% N_2O, GHSV = 45,000 h^{-1}	275	[53]
Cs-Co_3O_4	5% N_2O, GHSV = 7000 h^{-1}	110	This work
Cs-Co_3O_4	0.25% N_2O, GHSV = 8500 h^{-1}	210	[54]
PbO_2|Co_3O_4	5% N_2O, GHSV = 7000 h^{-1}	195	This work
PbO_2|Co_3O_4	0.2% N_2O, GHSV = 20,000 h^{-1}	180	[21]
CeO_2|Co_3O_4	5% N_2O, GHSV = 7000 h^{-1}	330	This work

In order to eliminate the ambiguities associated with various test conditions for reliable evaluation of the three discussed classes of cobalt spinel *s*-, *p*-, *d*-doping the results of deN_2O catalytic screening tests are shown in Figure 8 for the same contact time (GHSV = 7000 h^{-1}) and N_2O level (5%/He). The obtained data are schematically presented in the form of arrows indicating that the positive and negative effects of cobalt spinel additives can be dramatically differentiated, depending on the recognized interactions between the spinel phase and the dopants. The reference half N_2O conversion temperature ($T_{50\%}$) for the bare cobalt spinel obtained via a typical precipitation method is about 400 °C. The observed increase or decrease in the catalyst activity, depicted as a shift in the $T_{50\%}$ parameter in Figure 8, can be explained by the chemical nature (*s*-, *p*-, *d*-cations) and location (surface, bulk, and interface) of the dopants. Metals such as Na, K, Cs, Rb, Sr, and Ba are acting as efficient dopants when located at the surface, exhibiting a strong positive effect on the spinel performance. Among the surface promoters, the most efficient are heavy alkali metals K, Rb, and Cs, decreasing the $T_{50\%}$ down to 200 °C. In general, elements recognized as bulk additives can be divided into two groups of redox (most frequently transition metal cations), and non-redox (*s*- and *p*-cations) dopants. Whereas the introduction of Ni, Cu, and Zn cations with a higher number of *d* electrons than Co improves the activity ($\Delta T_{50\%}$ reaching 60 °C), incorporation into the Co_3O_4 structure cations with an inferior number of the *d* electrons like Mn or Fe leads to an increase of $T_{50\%}$ parameter (Figure 5, arrows pointing to the right). This observation implies the role of e_g electrons in the N_2O decomposition mechanism, similar to the case of the OER (Oxygen Evolution Reaction) process, where such an effect is well-documented [55]. It should be also mentioned that apart from the chemical nature of the dopants (*d*-electron configuration) their preference into tetrahedral vs. octahedral sites (ruled by the crystal field stabilization to a large extent) is another parameter to be taken into account. Based on the obtained results for several cations introduced into the spinel bulk, it may be concluded that the best

performance in the deN_2O reaction is linked with the chemical composition of the spinel octahedral sub-lattice. The location of the dopant is particularly crucial in the case of the non-redox dopants. Whereas substitution of the tetrahedral cobalt cations (e.g., by Mg) has rather a small effect of the catalytic activity, replacement of the octahedral ones (e.g., by Al) leads to a dramatic loss of spinel catalyst performance [39].

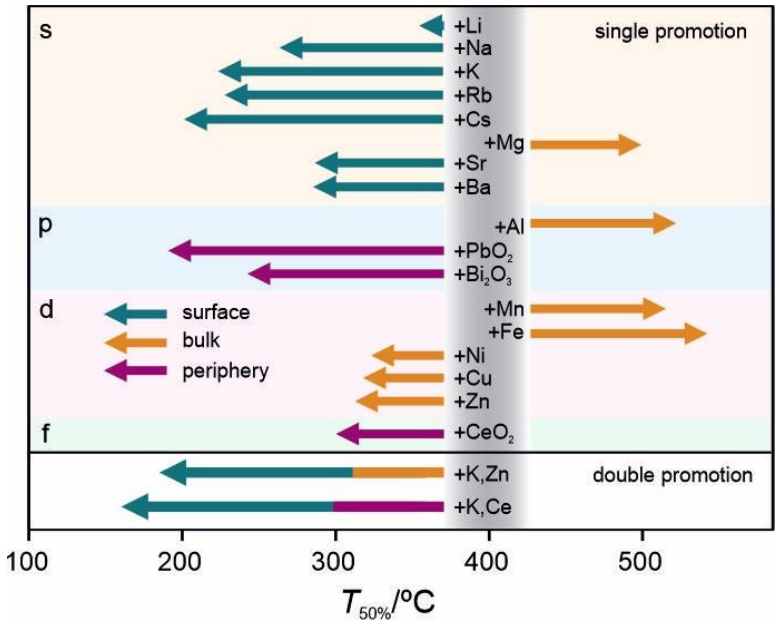

Figure 8. The deN_2O performance of Co_3O_4-doped phases compared by $T_{50\%}$ parameter (catalytic test conditions: a mixture of gases 5% N_2O/He, GHSV = 7000 h^{-1}).

The cerium, lead and bismuth oxides used as spinel admixtures can be classified as heterojunction promoters constituting separate phases where the interface between the oxides plays a crucial role in the catalytic mechanism of deN_2O reaction [21,22,56,57]. As reported by Grzybek et al., the catalytic activity of Co_3O_4|CeO_2 is controlled by the length of the periphery between these two phases [48].

The different origins of the promotional effects associated with the different dopant locations (surface, bulk, interface) are graphically summarized in Figure 9. Owing to their different space occupation, the synergetic or additive effects of the promoters can be achieved by their appropriate combinations [58]. Indeed, the results of the double promoted cobalt spinel-based catalysts (Figure 8, lower panel) clearly illustrate the beneficial effects of the combined surface/bulk (K-Zn) and surface/interface (K-Ce) promotion.

Figure 9. Graphical presentation of the promotional effects of cobalt spinel in terms of various localization of dopants.

4. Materials and Methods

4.1. Co_3O_4—Based Promoted Catalysts

A series of bulk-promoted catalysts were obtained by the co-precipitation method, using the mixture of cobalt and dopant nitrates with their appropriate concentration ratio. As a precipitation agent, the ammonia carbonate solution (1 M) was used. The precipitation was carried out until pH > 8.6, then the solid was filtered until pH = 7, dried at 100 °C for 12 h and calcined at 600 °C for 4 h. In the case of Mg- and Al-doped cobalt spinel catalysts, a higher temperature of calcination (900 °C) was applied in order to ensure the stability of the catalyst during the whole temperature range of the deN_2O activity test.

A series of alkali-promoted catalysts were prepared via incipient wetness impregnation method. The cobalt spinel phase, obtained by the precipitation method, was impregnated by the alkali (Li, Na, K, Rb or Cs) salts (nitrate, carbonate, acetate) or hydroxide solutions, with their concentrations providing the spinel surface coverage in the range of 0–8 atoms nm^{-2}. Then the samples were dried (100 °C/1 h) and calcined (500 °C/4 h).

4.2. Catalyst Characterization

The crystalline structure of the studied catalysts was investigated by means of XRD measurements. The data were collected on the Rigaku MiniFlex instrument with CuKα radiation (λ = 1.540598 Å), in the 2-theta range of 10–90° with the step of 0.02°. Additionally, phase characterization was carried out by Raman spectroscopy measurements. Spectra were collected in the room temperature by using Renishaw InVia spectrometer equipped with a Leica DMLM confocal microscope and a CCD detector with an excitation wavelength of 785 nm. The signal was registered in the range of 100–900 cm^{-1} and 10 consecutive scans were accumulated in order to obtained sufficient signal to noise ratio value. Specific surface area (SSA) of the reference sample and the bulk-promoted catalyst was determined by means of the N_2 adsorption and desorption measurements. The samples were outgassed (vacuum, 623 K/12 h) and the experiment was carried out at 77 K, using an ASAP 2010 Micromeritics instrument.

The reducibility of the obtained catalysts was investigated by H_2-TPR tests. Experiments were carried out in a quartz flow reactor with sintered glass, in the flow of the gas mixture 5% H_2/Ar and the temperature range between 20–800 °C. Every investigated sample was prepared in the form of a sieve fraction (0.2–0.3 mm grains). The signal was registered by Hiden Analytical QMS detector. Every sample was priory heated in the flow of helium at 500 °C.

For the catalyst surface composition, the X-ray photoelectron spectra technique was applied. The measurements were carried out by means of the Prevac spectrometer with a hemispherical VG SCIENTA R3000 analyzer. The data were collected with a pass energy of 100 eV for the survey and narrow scans, by using a monochromatized AlKα source (E = 1486.6 eV), and the electron flood gun (FS40A-PS). Obtained results were processed in CasaXPS software, where the carbon C1 t 284.8 eV peak was used as a reference.

Transmission electron microscopy (TEM) measurements were carried out using a Tecnai Osiris instrument (FEI) operating at 200 kV. Prior to TEM analysis, the samples were ultrasonically dispersed in methanol on a holey carbon film supported on a copper grid (400 mesh). The grid was dried for 45 min, and then surface contaminations were removed by plasma-cleaning (Solarus Gatan 950). All of the simulation and experimental details are provided in a previous paper [33].

The catalyst work function (Φ_{cat}), minimal energy needed to remove the electron from the catalyst surface to the vacuum energy level [46], was investigated under vacuum conditions (10^{-7} mbar). Catalysts were pelletized (10 mm of diameter, 8 MPa) and standardized by heating at 400 °C for 15 min before the measurements, which were done after cooling the sample to 150 °C. The measurements of the contact potential difference (V_{CPD}) were carried out by the Kelvin dynamic condenser method with the use of the KP6500 probe (McAllister Technical Services). As a reference, a standard stainless

steel electrode with a plate of 3 mm diameter (Φ_{ref} = 4.1 eV) was used. The values of the catalyst work function were determined following the equation: $\Phi_{cat} = \Phi_{ref} - V_{CPD}$.

4.3. N_2O Decomposition Tests

The catalytic tests of the obtained catalysts were carried out in the temperature-programmed surface reaction (TPSR) mode. For the experiments, 300 mg of the sieve fraction (0.2–0.3) of the catalyst was placed on the sintered glass of a quartz flow reactor. The deN_2O performance was investigated in the model feed of 5% N_2O/He in the flow of 30 mL/min (GHSV ≈ 7000 h^{-1}). The composition of gas-phase was constantly monitored by means of the QMS RGA200, SRS, where following m/z lines: 44 (N_2O), 32 (O_2), 28 (N_2), 18 (H_2O) were analyzed.

The experimental data of deN_2O tests were expressed as a conversion (X_{N2O}) versus temperature. Furthermore, in order to determine the activation energy, the kinetic model for the flow reactor with quasi ideal mixing was used and the Arrhenius formula was applied for this purpose.

5. Conclusions

The catalytic performance of the cobalt spinel in N_2O decomposition has been modified through promotion with *s*-, *p*-, *d*- and *f*-cations and screen at the same conditions. The localization at the surface, bulk or spinel-dopant interface of the additives allows for classifications and validation of the promotional effects. The reactivity descriptors such as catalyst work function, loading, and localization of dopants as well as their redox vs. non-redox nature were identified and used to guide the rational catalyst design. It has been found that among the examined dopants the most active are the alkali promoters located at the surface and those forming a spinel|reducible oxide interface (Co_3O_4|CeO_2, Co_3O_4|PbO_2). It was shown that the various promotional effects can be combined for efficient enhancement of cobalt spinel catalyst activity in the low-temperature N_2O decomposition.

Author Contributions: Conceptualization, Z.S. and A.K.; Data curation, S.W.; Formal analysis, G.G. and P.S.; Investigation, S.W., G.G. and P.S.; Methodology, Z.S. and A.K.; Supervision, A.K.; Visualization, S.W., G.G. and P.S.; Writing—original draft, S.W.; Writing—review & editing, G.G., P.S., Z.S. and A.K. All authors have read and agreed to the published version of the manuscript.

Funding: The authors would like to acknowledge the funding awarded by the Polish National Science Center (decision number 2017/27/B/ST4/01155). Sylwia Wójcik received funding for the preparation of her doctoral dissertation from the Polish National Science Center under the doctoral scholarship funding program (decision number 2019/32/T/ST4/00185).

Conflicts of Interest: The authors declare no conflicts of interest.

References

1. Rico-Pérez, V.; De Lecea, C.S.M.; Bueno-López, A. Preparation of $RhO_x/Ce_yPr_{1-y}O_2$ N_2O decomposition catalysts by rhodium nitrate impregnation with different solvents. *Appl. Catal. A Gen.* **2014**, *472*, 134–142. [CrossRef]
2. Zabilskiy, M.; Djinović, P.; Tchernychova, E.; Tkachenko, O.P.; Kustov, L.M.; Pintar, A. Nanoshaped CuO/CeO_2 Materials: Effect of the Exposed Ceria Surfaces on Catalytic Activity in N_2O Decomposition Reaction. *ACS Catal.* **2015**, *5*, 5357–5365. [CrossRef]
3. Obalová, L.; Pacultová, K.; Balabánová, J.; Jirátová, K.; Bastl, Z.; Valášková, M.; Lacný, Z.; Kovanda, F. Effect of Mn/Al ratio in Co-Mn-Al mixed oxide catalysts prepared from hydrotalcite-like precursors on catalytic decomposition of N_2O. *Catal. Today* **2007**, *119*, 233–238. [CrossRef]
4. Santiago, M.; Pérez-Ramírez, J. Decomposition of N_2O over hexaaluminate catalysts. *Environ. Sci. Technol.* **2007**, *41*, 1704–1709. [CrossRef]
5. Rutkowska, M.; Chmielarz, L.; Macina, D.; Piwowarska, Z.; Dudek, B.; Adamski, A.; Witkowski, S.; Sojka, Z.; Obalová, L.; Van Oers, C.J.; et al. Catalytic decomposition and reduction of N_2O over micro-mesoporous materials containing Beta zeolite nanoparticles. *Appl. Catal. B Environ.* **2014**, *146*, 112–122. [CrossRef]

6. Konsolakis, M. Recent Advances on Nitrous Oxide (N_2O) Decomposition over Non-Noble-Metal Oxide Catalysts: Catalytic Performance, Mechanistic Considerations, and Surface Chemistry Aspects. *ACS Catal.* **2015**, *5*, 6397–6421. [CrossRef]
7. Pietrogiacomi, D.; Campa, M.C.; Carbone, L.R.; Tuti, S.; Occhiuzzi, M. N_2O decomposition on CoO_x, CuO_x, FeO_x or MnO_x supported on ZrO_2: The effect of zirconia doping with sulfates or K^+ on catalytic activity. *Appl. Catal. B Environ.* **2016**, *187*, 218–227. [CrossRef]
8. Klegova, A.; Inayat, A.; Indyka, P.; Gryboś, J.; Sojka, Z.; Pacultová, K.; Schwieger, W.; Volodarskaja, A.; Kuśtrowski, P.; Rokicińska, A.; et al. Cobalt mixed oxides deposited on the SiC open-cell foams for nitrous oxide decomposition. *Appl. Catal. B Environ.* **2019**, *255*, 117745. [CrossRef]
9. Inayat, A.; Ayoub, M.; Abdullah, A.Z.; Ullah, S.; Naqvi, S.R. Decomposition of N_2O at low temperature over Co_3O_4 prepared by different methods. *Environ. Prog. Sustain. Energy* **2019**, *38*, 13129. [CrossRef]
10. Grzybek, G.; Wójcik, S.; Ciura, K.; Gryboś, J.; Indyka, P.; Oszajca, M.; Stelmachowski, P.; Witkowski, S.; Inger, M.; Wilk, M.; et al. Influence of preparation method on dispersion of cobalt spinel over alumina extrudates and the catalyst deN_2O activity. *Appl. Catal. B Environ.* **2017**, *210*, 34–44. [CrossRef]
11. Chromčáková, Ž.; Obalová, L.; Kovanda, F.; Legut, D.; Titov, A.; Ritz, M.; Fridrichová, D.; Michalik, S.; Kuśtrowski, P.; Jirátová, K. Effect of precursor synthesis on catalytic activity of Co_3O_4 in N_2O decomposition. *Catal. Today* **2015**, *257*, 18–25. [CrossRef]
12. Russo, N.; Fino, D.; Saracco, G.; Specchia, V. N_2O catalytic decomposition over various spinel-type oxides. *Catal. Today* **2007**, *119*, 228–232. [CrossRef]
13. Stelmachowski, P.; Maniak, G.; Kotarba, A.; Sojka, Z. Strong electronic promotion of Co_3O_4 towards N_2O decomposition by surface alkali dopants. *Catal. Commun.* **2009**, *10*, 1062–1065. [CrossRef]
14. Gudyka, S.; Grzybek, G.; Gryboś, J.; Indyka, P.; Leszczyński, B.; Kotarba, A.; Sojka, Z. Enhancing the deN_2O activity of the supported $Co_3O_4|\alpha$-Al_2O_3 catalyst by glycerol-assisted shape engineering of the active phase at the nanoscale. *Appl. Catal. B Environ.* **2017**, *201*, 339–347. [CrossRef]
15. Zasada, F.; Piskorz, W.; Sojka, Z. Cobalt Spinel at Various Redox Conditions: DFT+U Investigations into the Structure and Surface Thermodynamics of the (100) Facet. *J. Phys. Chem. C* **2015**, *119*, 19180–19191. [CrossRef]
16. Pacultová, K.; Karásková, K.; Kovanda, F.; Jirátová, K.; Šrámek, J.; Kustrowski, P.; Kotarba, A.; Chromčáková, Z.; Kočí, K.; Obalová, L. K-Doped Co-Mn-Al Mixed Oxide Catalyst for N_2O Abatement from Nitric Acid Plant Waste Gases: Pilot Plant Studies. *Ind. Eng. Chem. Res.* **2016**, *55*, 7076–7084. [CrossRef]
17. Dou, Z.; Zhang, H.; Pan, Y.; Xu, X. Catalytic decomposition of N_2O over potassium-modified Cu-Co spinel oxides. *J. Fuel Chem. Technol.* **2014**, *42*, 238–245. [CrossRef]
18. Maniak, G.; Stelmachowski, P.; Stanek, J.J.; Kotarba, A.; Sojka, Z. Catalytic properties in N_2O decomposition of mixed cobalt-iron spinels. *Catal. Commun.* **2011**, *15*, 127–131. [CrossRef]
19. Inger, M.; Wilk, M.; Saramok, M.; Grzybek, G.; Grodzka, A.; Stelmachowski, P.; Makowski, W.; Kotarba, A.; Sojka, Z. Cobalt spinel catalyst for N_2O abatement in the pilot plant operation-long-term activity and stability in tail gases. *Ind. Eng. Chem. Res.* **2014**, *53*, 10335–10342. [CrossRef]
20. Abu-Zied, B.M.; Soliman, S.A.; Abdellah, S.E. Pure and Ni-substituted Co_3O_4 spinel catalysts for direct N_2O decomposition. *Chin. J. Catal.* **2014**, *35*, 1105–1112. [CrossRef]
21. Yu, H.; Tursun, M.; Wang, X.; Wu, X. $Pb_{0.04}Co$ catalyst for N_2O decomposition in presence of impurity gases. *Appl. Catal. B Environ.* **2016**, *185*, 110–118. [CrossRef]
22. Tursun, M.; Wang, X.; Zhang, F.; Yu, H. Bi-Co_3O_4 catalyzing N_2O decomposition with strong resistance to CO_2. *Catal. Commun.* **2015**, *65*, 1–5. [CrossRef]
23. Abu-Zied, B.M.; Asiri, A.M. The role of alkali promoters in enhancing the direct N_2O decomposition reactivity over NiO catalysts. *Chin. J. Catal.* **2015**, *36*, 1837–1845. [CrossRef]
24. Grzybek, G.; Wójcik, S.; Indyka, P.; Ciura, K.; Sojka, Z.; Kotarba, A. Optimization of cesium and potassium promoter loading in alkali-doped $Zn_{0.4}Co_{2.6}O_4|Al_2O_3$ catalysts for N_2O abatement. *React. Kinet. Mech. Catal.* **2017**, *121*, 645–655.
25. Abu-Zied, B.; Bawaked, S.; Kosa, S.; Schwieger, W.; Abu-Zied, B.M.; Bawaked, S.M.; Kosa, S.A.; Schwieger, W. Rare Earth-Promoted Nickel Oxide Nanoparticles as Catalysts for N_2O Direct Decomposition. *Catalysts* **2016**, *6*, 70. [CrossRef]

26. Li, S.; Xia, L.; Li, J.; Liu, X.; Sun, J.; Wang, H.; Chi, Y.; Li, C.; Song, Y. Effect of alkaline earth metal doping on the catalytic performance of cobalt-based spinel composite metal oxides in N_2O decomposition. *J. Fuel Chem. Technol.* **2018**, *46*, 1377–1385. [CrossRef]
27. Yu, H.; Wang, X.; Li, Y. Strong impact of cobalt distribution on the activity for $Co_3O_4/CaCO_3$ catalyzing N_2O decomposition. *Catal. Today* **2020**, *339*, 274–280. [CrossRef]
28. Maniak, G.; Stelmachowski, P.; Zasada, F.; Piskorz, W.; Kotarba, A.; Sojka, Z. Guidelines for optimization of catalytic activity of 3d transition metal oxide catalysts in N_2O decomposition by potassium promotion. *Proc. Catal. Today Elsevier* **2011**, *176*, 369–372. [CrossRef]
29. Maniak, G.; Stelmachowski, P.; Kotarba, A.; Sojka, Z.; Rico-Pérez, V.; Bueno-López, A. Rationales for the selection of the best precursor for potassium doping of cobalt spinel based deN2O catalyst. *Appl. Catal. B Environ.* **2013**, *136–137*, 302–307. [CrossRef]
30. Obalová, L.; Maniak, G.; Karásková, K.; Kovanda, F.; Kotarba, A. Electronic nature of potassium promotion effect in Co-Mn-Al mixed oxide on the catalytic decomposition of N_2O. *Catal. Commun.* **2011**, *12*, 1055–1058. [CrossRef]
31. Grzybek, G.; Wójcik, S.; Legutko, P.; Gryboś, J.; Indyka, P.; Leszczyński, B.; Kotarba, A.; Sojka, Z. Thermal stability and repartition of potassium promoter between the support and active phase in the $K\text{-}Co_{2.6}Zn_{0.4}O_4|\alpha\text{-}Al_2O_3$ catalyst for N_2O decomposition: Crucial role of activation temperature on catalytic performance. *Appl. Catal. B Environ.* **2017**, *205*, 597–604. [CrossRef]
32. Zasada, F.; Kaczmarczyk, J.; Indyka, P.; Sojka, Z.; Kotarba, A.; Piskorz, W.; Janas, J. Thermodynamic Stability, Redox Properties, and Reactivity of Mn_3O_4, Fe_3O_4, and Co_3O_4 Model Catalysts for N_2O Decomposition: Resolving the Origins of Steady Turnover. *ACS Catal.* **2016**, *6*, 1235–1246.
33. Zasada, F.; Gryboś, J.; Indyka, P.; Piskorz, W.; Kaczmarczyk, J.; Sojka, Z. Surface structure and morphology of M[CoM'] O_4 (M = Mg, Zn, Fe, Co and M' = Ni, Al, Mn, Co) spinel nanocrystals-DFT+U and TEM screening investigations. *J. Phys. Chem. C* **2014**, *118*, 19085–19097. [CrossRef]
34. Lavina, B.; Salviulo, G.; Della Giusta, D. Cation distribution and structure modelling of spinel solid solutions. *Phys. Chem. Miner.* **2002**, *29*, 10–18. [CrossRef]
35. Hill, R.J.; Craig, J.R.; Gibbs, G.V. Systematics of the spinel structure type. *Phys. Chem. Miner.* **1979**, *4*, 317–339. [CrossRef]
36. Kim, J.-G.; Pugmire, D.L.; Battaglia, D.; Langell, M.A. Analysis of the $NiCo_2O_4$ spinel surface with Auger and X-ray photoelectron spectroscopy. *Appl. Surf. Sci.* **2000**, *165*, 70–84. [CrossRef]
37. Li, Y.; Wang, X. MgO Modifying Al_2O_3 to Load Cobalt Oxide for Catalytic N_2O Decomposition. *Catal. Lett.* **2019**, *149*, 1856–1863. [CrossRef]
38. Ivanova, Y.A.; Sutormina, E.F.; Isupova, L.A.; Rogov, V.A. Effect of the Composition of $Ni_xCo_{3-x}O_4$ (x = 0-0.9) Oxides on Their Catalytic Activity in the Low-Temperature Reaction of N_2O Decomposition. *Kinet. Catal.* **2018**, *59*, 365–370. [CrossRef]
39. Stelmachowski, P.; Maniak, G.; Kaczmarczyk, J.; Zasada, F.; Piskorz, W.; Kotarba, A.; Sojka, Z. Mg and Al substituted cobalt spinels as catalysts for low temperature deN_2O-Evidence for octahedral cobalt active sites. *Appl. Catal. B Environ.* **2014**, *146*, 105–111. [CrossRef]
40. Stelmachowski, P.; Ciura, K.; Grzybek, G. Morphology-dependent reactivity of cobalt oxide nanoparticles in N2O decomposition. *Catal. Sci. Technol.* **2016**, *6*, 5554–5560. [CrossRef]
41. Zasada, F.; Gryboś, J.; Budiyanto, E.; Janas, J.; Sojka, Z. Oxygen species stabilized on the cobalt spinel nano-octahedra at various reaction conditions and their role in catalytic CO and CH_4 oxidation, N_2O decomposition and oxygen isotopic exchange. *J. Catal.* **2019**, *371*, 224–235. [CrossRef]
42. Grzybek, G.; Stelmachowski, P.; Gudyka, S.; Duch, J.; Ćmil, K.; Kotarba, A.; Sojka, Z. Insights into the twofold role of Cs doping on deN2O activity of cobalt spinel catalyst-towards rational optimization of the precursor and loading. *Appl. Catal. B Environ.* **2015**, *168–169*, 509–514. [CrossRef]
43. Abu-Zied, B.M.; Soliman, S.A.; Asiri, A.M. Role of rubidium promotion on the nitrous oxide decomposition activity of nanocrystalline $Co_3O_4\text{-}CeO_2$ catalyst. *Appl. Surf. Sci.* **2019**, *479*, 148–157. [CrossRef]
44. Kapteijn, F.; Rodriguez-Mirasol, J.; Moulijn, J.A. Heterogeneous catalytic decomposition of nitrous oxide. *Appl. Catal. B Environ.* **1996**, *9*, 25–64. [CrossRef]
45. Tolman, W.B. Binding and activation of N_2O at transition-metal centers: Recent mechanistic insights. *Angew. Chem. Int. Ed.* **2010**, *49*, 1018–1024. [CrossRef]

46. Somorjai, G.A.; Li, Y. *Introduction to Surface Chemistry and Catalysis*; Wiley: Hoboken, NJ, USA, 2010; ISBN 9780470508237.
47. Zasada, F.; Stelmachowski, P.; Maniak, G.; Paul, J.F.; Kotarba, A.; Sojka, Z. Potassium promotion of cobalt spinel catalyst for N_2O decomposition-accounted by work function measurements and DFT modelling. *Catal. Lett.* **2009**, *127*, 126–131. [CrossRef]
48. Grzybek, G.; Gudyka, S.; Stelmachowski, P.; Rico-Pérez, V.; Indyka, P.; Guillén-Hurtado, N.; Bueno-López, A.; Kotarba, A.; Sojka, Z. Strong dispersion effect of cobalt spinel active phase spread over ceria for catalytic N2O decomposition: The role of the interface periphery. *Appl. Catal. B Environ.* **2015**, *180*, 622–629. [CrossRef]
49. Wójcik, S.; Indyka, P.; Sojka, Z.; Kotarba, A. Development of structured Co_3O_4-based catalyst for N_2O removal from hospital ventilation systems. *Catal. Today* 2019. [CrossRef]
50. You, Y.; Chang, H.; Ma, L.; Guo, L.; Qin, X.; Li, J.; Li, J. Enhancement of N_2O decomposition performance by N_2O pretreatment over Ce-Co-O catalyst. *Chem. Eng. J.* **2018**, *347*, 184–192. [CrossRef]
51. Yan, L.; Ren, T.; Wang, X.; Gao, Q.; Ji, D.; Suo, J. Excellent catalytic performance of $Zn_xCo_{1-x}Co_2O_4$ spinel catalysts for the decomposition of nitrous oxide. *Catal. Commun.* **2003**, *4*, 505–509. [CrossRef]
52. Amrousse, R.; Chang, P.-J.; Choklati, A.; Friche, A.; Rai, M.; Bachar, A.; Follet-Houttemane, C.; Hori, K. Catalytic decomposition of N_2O over Ni and Mg-magnetite catalysts. *Catal. Sci. Technol.* **2013**, *3*, 2288–2294. [CrossRef]
53. Kim, M.J.; Lee, S.J.; Ryu, I.S.; Moon, S.H.; Jeon, M.W.; Ko, C.H.; Jeon, S.G. Understanding the Effect of NO Adsorption on Potassium-Promoted Co_3O_4 for N_2O Decomposition. *Catal. Lett.* **2017**, *147*, 2886–2892. [CrossRef]
54. Pasha, N.; Lingaiah, N.; Babu, N.S.; Reddy, P.S.S.; Prasad, P.S.S. Studies on cesium doped cobalt oxide catalysts for direct N_2O decomposition in the presence of oxygen and steam. *Catal. Commun.* **2008**, *10*, 132–136. [CrossRef]
55. Su, D.; Dou, S.X.; Wang, G. Single crystalline Co_3O_4 nanocrystals exposed with different crystal planes for Li-o2 batteries. *Sci. Rep.* **2014**, *4*, 5767. [CrossRef]
56. Xiong, S.; Chen, J.; Huang, N.; Yang, S.; Peng, Y.; Li, J. Balance between Reducibility and N_2O Adsorption Capacity for the N_2O Decomposition: CuxCoy Catalysts as an Example. *Environ. Sci. Technol.* **2019**, *53*, 10379–10386. [CrossRef]
57. Wang, Y.; Zheng, K.; Hu, X.; Zhou, W.; Wei, X.; Zhao, Y. Y_2O_3 promoted Co_3O_4 catalyst for catalytic decomposition of N_2O. *Mol. Catal.* **2019**, *470*, 104–111. [CrossRef]
58. Ivanova, Y.A.; Sutormina, E.F.; Isupova, I.A.; Vovk, E.I. Catalytic Activity of the Oxide Catalysts Based on $Ni_{0.75}Co_{2.25}O_4$ Modified with Cesium Cations in a Reaction of N_2O Decomposition. *Kinet. Catal.* **2017**, *58*, 773–779. [CrossRef]